

1 **Biobased additives for asphalt applications produced from**
2 **the hydrothermal liquefaction of sewage sludge**

3 Diego López Barreiro¹, Francisco J. Martin-Martinez^{1,4}, Shengfei Zhou¹, Ixone Sagastagoia²,
4 Francisco del Molino Pérez², Francisco Javier Arrieta Morales², Markus J. Buehler^{1,3*}

5 *¹Department of Civil and Environmental Engineering, Massachusetts Institute of Technology, 77*
6 *Massachusetts Ave., Cambridge, MA 02139, USA*

7 *²R&D Department, Cadagua, Gran Vía, 45, 48011 Bilbao, Vizcaya, Spain*

8 *³Center for Computational Science and Engineering, Schwarzman College of Computing,*
9 *Massachusetts Institute of Technology, 77 Massachusetts Ave., Cambridge, MA 02139, USA*

10 *⁴Department of Chemistry, Swansea University, SAI 8PP, Swansea, UK*

11 **corresponding author, mbuehler@MIT.EDU and +1.617.452.2750*

12

13 **ABSTRACT**

14 Sewage sludge from wastewater treatment plants is a large source of organic waste with
15 suboptimal disposal solutions available. Current handling solutions include disposing of it as
16 fertilizer on arable land, or direct discharge in the sea. This work investigates the valorization
17 of sewage sludge into biocrude oils using hydrothermal liquefaction (HTL). Biocrude oils are
18 bitumen-like materials with potential applications as green additives for asphalt binder, one of
19 the most used materials in infrastructure. This work investigates links between feedstock
20 (digested *versus* non-digested sludge), HTL conditions (temperature, biomass loading to the
21 reactor and reaction time) and yields of biocrude oils from sewage sludge. Our data suggests
22 that non-digested sewage sludge leads to higher biocrude oil yields (30-40 wt %) at
23 temperatures of 300-320 °C and biomass loadings of 20 wt %. Furthermore, we use density
24 functional theory (DFT) calculations to study the reactivity and clustering mechanisms of
25 asphaltenes – a key molecular component of asphalt binder, and largely responsible of its
26 mechanical performance. Biobased asphaltenes are present in biocrude oil, and our aim was to
27 understand their differences with fossil asphaltenes derived from petroleum. Our data suggests
28 that biobased asphaltenes are similar to petroleum-based ones in terms of thermodynamic
29 stability and π - π stacking, despite the higher content in polar chemical functionalities in
30 biobased asphaltenes. Overall, the chemical features and intermolecular interactions indicate
31 that biocrude oils produced from sewage sludge via HTL are promising candidates for
32 application as asphalt additives.

33 **KEYWORDS:** Biocrude oil; hydrothermal liquefaction; DFT; asphalt; sewage sludge

34

35

36

37

38 1. INTRODUCTION

39 Sewage sludge is a large source of biowaste generated in wastewater treatment plants
40 (WWTPs) [1,2]. Globally, more than 330 km³ of municipal wastewater are produced yearly
41 [3]. It is estimated that 60% of the produced municipal wastewater is treated in WWTPs,
42 leading to the production of vast amounts of sewage sludge worldwide. Annually, 50 million
43 tons of sludge (water content of ca. 80%) are produced in the EU, while the USA and China
44 account for approximately 40 million tons each [1]. This represents an enormous organic waste
45 source that is currently underutilized and that represents an environmental issue with no clear
46 solution to the present. Current handling approaches are dissipative, costly (up to 50% of total
47 operating costs in WWTPs [1]) and generate no or little value. Conventional WWTPs produce
48 two types of sewage sludge: primary and secondary sludge. These can be mixed and stabilized
49 through anaerobic digestion to partially convert it into biogas, a gaseous mixture containing
50 methane (CH₄), carbon dioxide (CO₂) and other gases (H₂, N₂, H₂S and O₂). The remaining
51 nondegradable solid fraction can be dried and disposed of as fertilizer due to its high content in
52 nutrients. However, this can lead to eutrophication and acidification effects, which have
53 triggered the implementation of strict regulations in several countries to limit the amount of
54 digestate used as field fertilizer [4]. Therefore, new applications for sewage sludge are urgently
55 needed. To that end, biocrude oil produced from the hydrothermal liquefaction (HTL) of
56 biomass has shown promising results as green additive for asphalt binders, one of the most
57 highly-demanded materials in infrastructure [5]. The vast majority of the roads are paved using
58 petroleum-based binders as the pitch that binds aggregate particles to create asphalt concrete
59 [6–8]. Nonetheless, the increasing cost of petroleum extraction and the environmental concerns
60 about the usage of fossil resources have encouraged the asphalt pavement industry to look for
61 additives and substitutes to petroleum-derived asphalt binders that simultaneously enhance
62 performance and sustainability [8–10].

63 Here, we investigate the HTL of sewage sludge to produce biocrude oil. HTL is a
64 thermochemical process that converts wet biomass (water content > 50 wt %), including algae,
65 manure, or sewage sludge, into biocrude oil [11–14]. Water remains in a liquid state during
66 HTL by applying subcritical conditions (280-350 °C, 10.0-22.1 MPa). This is energy-efficient
67 for feedstocks like sewage sludge, because it allows to process the biomass together with the
68 water naturally present in it. This represents a high energy saving when compared to other
69 thermochemical processes like pyrolysis, because the energy-intensive step of evaporating
70 water is avoided [15,16]. In fact, water under HTL conditions displays very different properties
71 to those commonly observed at standard conditions [15,16], including high availability of
72 hydronium and hydroxyl ions, lower density or lower conductivity. Moreover, water acts as a
73 reactant during HTL, hydrolyzing and degrading the biomass biopolymers (e.g., cellulose,
74 hemicellulose, lignin, or proteins) to form biocrude oil. Several studies have indicated that
75 HTL has a positive balance in terms of economics and sustainability when applied to sewage
76 sludge [17,18]. However, these and other studies on biocrude oils obtained via HTL have
77 mostly focused on biofuel applications. To that end, HTL converts all biomass fractions to
78 biocrude oil [15], conversely to other biofuel production processes that only utilize a certain
79 biomass fraction (e.g., lipids for biodiesel, or carbohydrates for bioethanol).

80 Recent research has demonstrated also the applicability of HTL biocrude oil from
81 microalgae [8,9,14], swine manure [14,19], or food waste [20] as asphalt additive. Reported
82 benefits of adding biocrude oils to asphalt mixes include antioxidant properties, aging retard,
83 lower temperature applicability and superior mechanical performance under working load
84 conditions [19–21]. The behavior of asphalt binders is linked to their molecular composition,
85 which is commonly described as a mixture of four classes of molecules: aromatics, saturates,
86 resins and asphaltenes. Specifically, asphaltenes (the focus of our computational work) are key
87 components for the mechanical performance of asphalt concrete. Asphaltenes tend to form

88 clusters and supramolecular nanoaggregates [22]. Their oxidative aging [14] leads to an
89 increase in the number and size of these nanoaggregates, which produces a macroscopic
90 hardening of asphalt pavement. This can trigger stress concentration and compromise its
91 mechanical performance [23]. Therefore, understating the aggregation of asphaltenes and their
92 reactivity (i.e., its tendency to engage in chemical reactions and the most reactive functional
93 groups in their structure) is relevant to develop strategies that prevent asphalt aging.

94 While there is a large body of research on fossil asphalt binders, which has led to the well-
95 known Yen-Mullins model for the description of asphalt's structure [22], the development of a
96 similar model for biocrude oils is still lacking. The Yen-Mullins model describes the
97 hierarchical structure of asphalt in which asphaltene nanoaggregates are embedded in a matrix
98 of lighter molecular structures (saturates, resins, and small aromatic molecules). In the Yen-
99 Mullins model, asphaltenes are described as single, moderate-sized polycyclic aromatic
100 hydrocarbons (PAHs) with peripheral alkane substitutions, i.e., aliphatic chains. In contrast,
101 much less is known about the asphaltene-like matter in biocrude oils. More details on the
102 molecular composition of biocrude oils, in combination with atomistic simulations, are needed.

103 The composition of biocrude oils is typically evaluated using techniques like
104 chromatography-mass spectrometry (GC-MS) [24]. This works well for the light, volatile
105 fraction of biocrude oil. However, the heavy components of biocrude oil (e.g. asphaltenes) are
106 non-volatile, and therefore not amenable to GC-MS [24]. Other techniques, such as or
107 thermogravimetric analysis (TGA), fail to provide a molecular picture with sufficient depth of
108 this fraction too [25]. Fortunately, our knowledge of the heavy fraction in biocrude oils has
109 increased in recent years [8,25,26], which has also enabled further advances in the
110 development of molecular models. To that end, our group provided an atomistic model for
111 HTL biocrude oils produced from microalgae slurries using pyrolysis-GC-MS [27]. Our data
112 suggested that a large fraction of biocrude oil (>65 wt %) was non-volatile at temperatures

113 below 280 °C, whereas asphaltene-like matter constituted up to 10-15 wt % of the biocrude oil
114 mass. These asphaltene-like molecules were mostly polycyclic aromatic structures [9,27]
115 analogous to fossil asphaltenes. Furthermore, conceptual DFT [28] calculations performed
116 using our atomistic model showed that asphaltenes in biocrude oil had the highest tendency
117 towards oxidation from all its compounds, an effect previously identified in fossil asphaltenes
118 too [29].

119 The yield of biocrude oils depend on the biomass feedstock and the HTL conditions
120 applied (i.e., temperature, reaction time, biomass loading to the reactor) [30]. Thus, it is
121 important to identify the feedstocks and processing conditions that can maximize the
122 production of fit-for-purpose biocrude oils that can be incorporated in the asphalt industry, i.e.,
123 the feedstock-processing-property relationships for biocrude oils. Here, we use HTL to produce
124 biocrude oil from non-digested and digested sewage sludge – i.e., before and after anaerobic
125 digestion. The sewage sludge type, biomass loading to the reactor and HTL temperature are
126 varied to assess the links between feedstock, HTL conditions, and biocrude oil yield.
127 Furthermore, unveiling how asphaltenes in biocrude oil behave at the nanoscale is critical to
128 understand their role as additives in the macroscopic mechanical properties of asphalt. To that
129 end, we compare here aggregates of fossil and biobased asphaltenes using DFT calculations,
130 with a focus on understanding the differences at the molecular level in terms of thermodynamic
131 stability and aggregation tendency.

132 **2. MATERIALS AND METHODS**

133 **2.1.Feedstock**

134 Non-digested and digested mixed sludges were obtained from the WWTP of Bens (A
135 Coruña, Spain) operated by Cadagua. Digested sludge was obtained from non-digested sludge
136 after an anaerobic digestion step. **Figure S1** shows the process diagram of a conventional
137 WWTP, highlighting in red the types of sludge used in this research. The sludges were dried at

138 105 °C until constant weight to remove water. The ash content was analyzed by subjecting 1 g
139 of dry sewage sludge to 550 °C for 5 h in a muffle furnace.

140 **2.2. Hydrothermal liquefaction (HTL)**

141 HTL experiments were carried out in a high pressure, high temperature reactor with a
142 volume of 75 mL (Parr Instrument Company Model 4740). Three temperatures (280, 300 and
143 320 °C), two biomass loadings to the reactor (10 wt % and 20 wt %), and two reaction times
144 (10 and 30 min) were tested for each sewage sludge type in this study. The temperature
145 selection was based on previous reports on the production of biocrude oils from biological
146 sources (including algae or hog manure) with promising rheological properties and chemical
147 compositions as asphalt additives [9,14,31]. Biomass loadings and reaction times were selected
148 based on recommended values for an economic HTL process [15].

149 The dry sludges were mixed with distilled water to form a slurry of 10 or 20 wt %. The
150 mass of slurry added to the reactor was calculated for each temperature in order to ensure that
151 sufficient pressure built up inside the reactor upon heating to keep water in a liquid state. For
152 each run, the reactor was tightly sealed and flushed 3 times with pure nitrogen (20 bar) to
153 remove the air from the reaction vessel. Subsequently, it was placed in a heating block, with a
154 temperature controller connected to a thermocouple located inside the reactor. The heating
155 period was ca. 35-45 min, depending on the final temperature. The start of the reaction time
156 was taken as the time at which the interior of the reactor attained a temperature 5 °C below the
157 set-point temperature. All the experiments were carried out at least in duplicate. After the
158 reaction time was completed, the reactor was submerged in a cold water bath for fast
159 quenching.

160 **2.3. HTL product separation**

161 Once the temperature inside the reactor reached room temperature, the pressure was
162 recorded and the gas vented. The mass of gas was calculated with the ideal gas law, using the

163 pressure inside the autoclave after the HTL experiment. It was assumed that the molar mass of
164 the gas was equal to that of CO₂, based on our own experience and the vast body of research
165 reporting that HTL gas is almost entirely (>98%) composed of CO₂ at the reaction conditions
166 used here [32,33]. The remaining HTL products inside the vessel (biocrude oil, aqueous phase
167 and hydrochar) were then separated. The aqueous product was separated by vacuum filtration
168 using glass microfiber filter (Whatman GF/B, 1 μm pore size). The hydrochar and biocrude oil
169 phases remained on the filter cake or stuck to the inner walls of the autoclave. To separate the
170 biocrude oil from the hydrochar, the autoclave interior and the filter cake were washed with
171 dichloromethane (DCM, Sigma-Aldrich, 99% purity). Stepwise additions of 5 mL of DCM
172 were used to maximize the recovery of biocrude oil. The mass of biocrude oil was calculated
173 after evaporating the DCM by flushing until constant weight with air to remove residual DCM
174 and water. The hydrochar remained on top of the filter and was dried at 105 °C overnight to
175 remove residual DCM and water and to determine its dry mass. Its ash content was determined
176 by treating it at 550 °C for 5 hours in a muffle furnace.

177 The mass yields of gas, biocrude oil and hydrochar were calculated on an organic basis as
178 the ratio of the weight of the recovered organic mass (m_i) and the dry, ash-free (daf) mass of
179 sewage sludge initially loaded to the reactor, according to **Equation 1**:

$$180 \quad \text{Yield (wt\%)} = \frac{m_i}{m_{\text{sewage sludge(daf)}}} \cdot 100 \quad (1)$$

181 The yield for the aqueous phase plus the mass losses during the HTL reaction and the
182 product separation were calculated as the difference between 100% and the yields of gas,
183 biocrude oil and hydrochar.

184 **2.4.Density Functional Theory (DFT)**

185 The minimum-energy geometry, the electron density, and several associated parameters
186 were calculated for model fossil and biobased asphaltene molecules (**Figure S2**) with DFT

187 methods as implemented in the ORCA 4.1.1 Computational package [34]. Three model fossil
188 asphaltenes proposed on earlier publications [35,36] were used for these simulations. These
189 asphaltenes have an island structure, which is the dominant molecular structure for these
190 compounds [37]. Biobased counterparts with a higher content of heteroatoms (N and O) and
191 slightly larger aromatic cores were taken from our earlier molecular model for biocrude oils
192 from microalgae [27]. Several literature examples show that biocrude oils from microalgae and
193 sewage sludge have similar molecular components (albeit in different concentrations),
194 elemental composition and thermal stability [2,11,38–40]. Thus, we considered these
195 molecules as representative of asphaltene-like matter in biocrude oil from sewage sludge.

196 DFT calculations were used to understand the differences in thermodynamic stability and
197 aggregation tendency for both types of asphaltenes. The Becke's hybrid exchange functional
198 with the Lee-Yang-Parr correlation functional (B3LYP) was used, together with the 6-31G*
199 basis set, which includes polarization functions. B3LYP/6-31G* is established as a good level
200 of theory for describing the geometry and electron density of organic molecules like the ones
201 considered here. Standard DFT functionals fail to describe dispersion forces [41], an essential
202 component in noncovalent interactions. Thus, Grimme's DFT-D3 approach [42] with Becke-
203 Johnson damping (D3BJ) [43] was implemented to correct the energies arising from dispersion
204 interactions. The basis set superposition error (BSSE) that occurs in non-covalent complexes as
205 a consequence of the overlapping of basis functions was also corrected by the geometric
206 counterpoise scheme (gCP) [44].

207 The initial molecular structures of fossil and biobased asphaltenes were subjected to
208 geometry optimization to obtain the most stable conformations. In-house Python scripts were
209 then used to automate the creation of asphaltene dimers using the minimum-energy structures
210 from the geometry optimization step, using different rotation angles between monomers (0, 30,
211 60 and 90 degrees). This was done to enhance the sampling of the conformational space and

212 prevent artefacts caused by the starting configuration of the dimer from affecting the results.
213 Only parallel π - π conformations were considered, as previous studies showed that these
214 configurations were energetically favored for asphaltene dimers [45]. The dimers were
215 optimized to study their binding energies and intermolecular distances d , in order to assess the
216 aggregation tendency of fossil *versus* biobased asphaltenes. Binding energies (E_{bind}) were
217 calculated as the difference in energy of the individual monomers with respect to the energy of
218 the dimer (**Equation 2**):

$$219 \quad E_{\text{bind}} = E_{\text{dimer}} - 2 \cdot E_{\text{monomer}} \quad (2)$$

220 E_{monomer} represents the total energy of asphaltene monomer, and E_{dimer} the total energy of
221 the asphaltene dimer (BSSE-corrected). For each dimer, we performed calculations using
222 model molecules with and without aliphatic side chains, to isolate the contribution of the
223 polycyclic aromatic core to the total binding energy and to evaluate the effect of the aliphatic
224 chains in the intermolecular distance and the π - π stacking. The asphaltenes cores were initially
225 placed at a distance of 4 Å for simulations without side chains, and 8 Å for simulations with
226 side chains.

227 In the framework of conceptual DFT [28], the differentiation of the energy (E) of a
228 molecular system with respect to the number of electrons is used to evaluate different reactivity
229 descriptors, i.e., second derivative-type reactivity descriptors (chemical hardness) and local
230 descriptors such as the Fukui function. The global chemical hardness (η) is formally defined as
231 the second derivative of the energy with respect to the number of electrons at fixed external
232 potential. In a practical way, η was calculated as the difference between the ionization energy
233 (I) and the electron affinity (A), following the same procedure reported elsewhere [27], in
234 which the Parr-Pearson description [46] adapted by Cardenas et al [47] was used (**Equation 3**).

$$235 \quad \eta = \frac{1}{2} (I - A) \quad (3)$$

236 The Fukui function can be interpreted as the change of the electron density when the total
237 number of electrons is changed. In practice, the dual descriptor of the Fukui function was
238 calculated by electron density differences between the neutral and the positively- and
239 negatively-charged molecules for each asphaltene, and plotted at isosurface values of 0.001
240 electron·bohr⁻³. VMD [48] was used for visualization. Aromatic rings in asphaltene cores were
241 colored attending to Cremer–Pople pucker amplitude values, which is a puckering spherical
242 coordinate system in which the radius Q means the magnitude of puckering, measuring the
243 deviation from a perfectly flat six-membered ring [49]. The values of Q obtained by this
244 method were color-coded by the PaperChain representation implemented in VMD.

245 3. RESULTS AND DISCUSSION

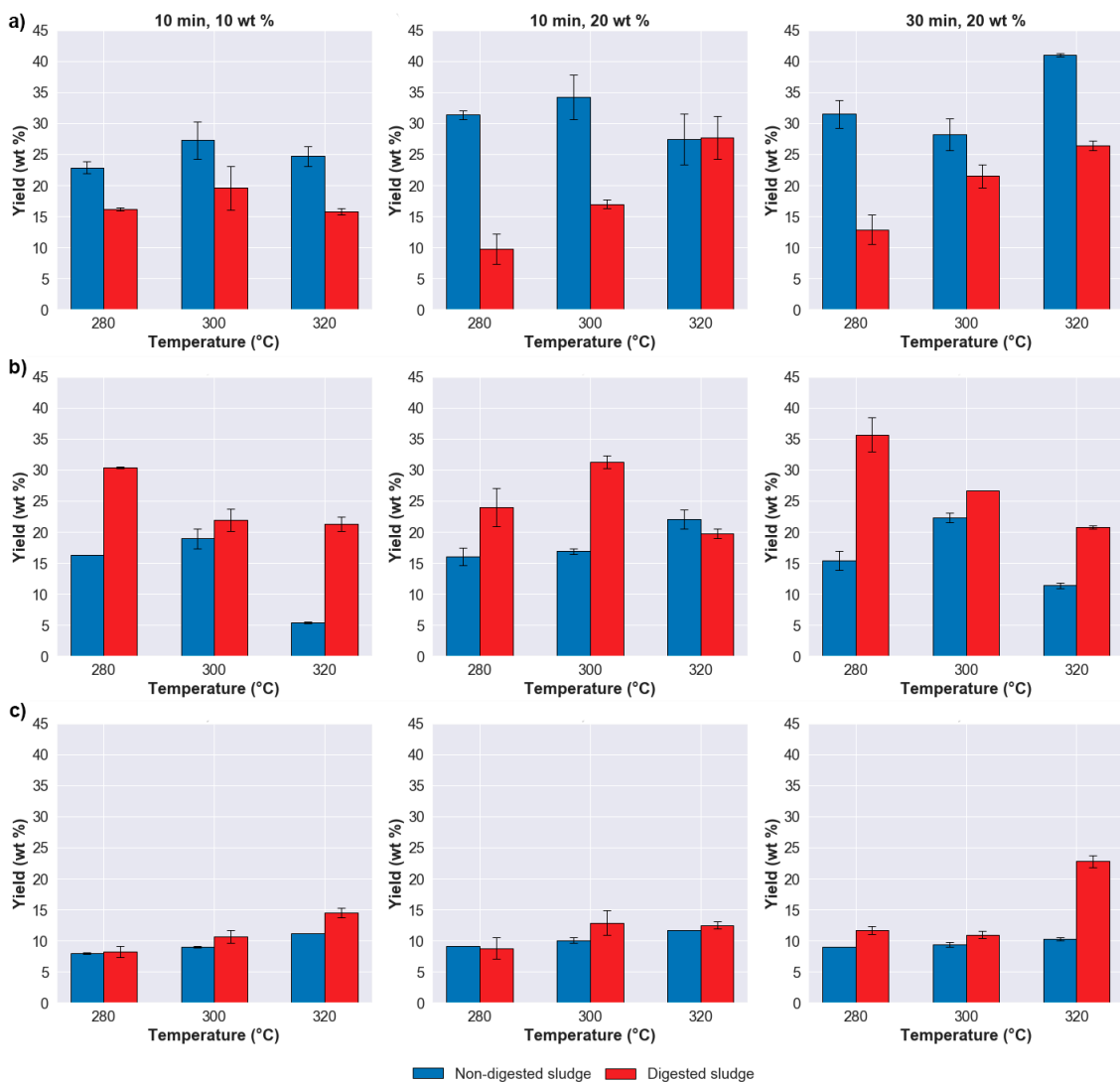
246 3.1. Effect of HTL parameters on the biocrude oil yield

247 **Table S1** reports the characterization of the feedstock. The ash content more than doubled
248 for digested sludge ($33.1 \pm 0.1\%$), compared to non-digested sludge ($15.3 \pm 0.2\%$). Since the
249 ash fraction is unaltered by the anaerobic digestion, this indicates that more than half of the
250 organic mass in non-digested sludge converted to biogas during the anaerobic digestion step.
251 **Figure 1** and **Table S2** summarizes the HTL product yields (dry, ash-free basis) for both types
252 of sludge at different temperatures, reaction times, and biomass loading to the reactor.
253 Generally, the biocrude oil yield in the HTL is controlled by a balance between biomass
254 decomposition reactions to form water-soluble organics (expected to dominate at short
255 residence times) and repolymerization reactions to form biocrude oil or hydrochar (expected to
256 dominate at extended residence times) [38,50]. The balance between these reactions is
257 determined by the parameters used during HTL (e.g., feedstock, temperature, biomass loading,
258 reaction time) [51], and the following sections dissect how those parameters affect the biocrude
259 oil yield. Overall, non-digested sludge led to higher biocrude oil yields for most of the
260 conditions tested. However, this does not necessarily mean that an industrial HTL process

261 integrated in a WWTP would be more efficient when using non-digested sludge as feedstock.
262 The energy gain from the biogas produced in the anaerobic digestion step (**Figure S1**) should
263 be considered in a techno-economic analyses to determine the optimal process configuration.

264 *Effect of the feedstock:* in most cases, non-digested sludge led to higher biocrude oil yields
265 than digested sludge. Only in experiments at 320 °C, 10 min, and 20 wt% loading the yields
266 became similar for both feedstocks (**Figure 1a**). Thus, non-digested sludge appeared as a more
267 amenable feedstock to HTL, while digested sludge had a higher tendency to form hydrochar
268 (**Figure 1b**). We attributed this to the more recalcitrant character of digested sludge, which
269 made it less prone to degradation under HTL conditions. Higher gas formation was observed
270 for experiments with digested sludge, an effect that was enhanced at higher HTL temperatures
271 (**Figure 1c**). This could be caused by the higher ash content of digested sludge (**Table S1**)
272 because many inorganic salts, including K_2CO_3 , KOH, $Ca_3(PO_4)_2$, $CaCO_3$ or $Ca(OH)_2$, are
273 known to catalyze the conversion of organic matter into gas during HTL [16,52–55]. A similar
274 behavior was previously observed for other biomass feedstocks, including microalgae [13],
275 lignin [56], or glucose [33].

276 *Effect of the temperature:* an increase in HTL temperature brought along an increase in the
277 gas yield, both for non-digested and digested sludge (**Figure 1c**). In contrast, the biocrude oil
278 yields exhibited a more irregular behavior (**Figure 1a**). In most of the reaction times and
279 biomass loadings tested, the highest biocrude oil yields for both feedstocks were obtained at
280 320 °C – although at different reaction times. However, under some HTL conditions, the
281 biocrude oil yield started to decline at 320 °C. Such a behavior was already observed for other
282 biomass feedstocks [57–59], and was attributed to an enhancement of gasification reactions
283 that convert biomass components into gaseous molecules (i.e., in the case of digested sludge at
284 30 min and 20 wt %), or repolymerization reactions that stimulate the formation of hydrochar
285 [50] (i.e., in the case of non-digested sludge at 10 min and 20 wt %).



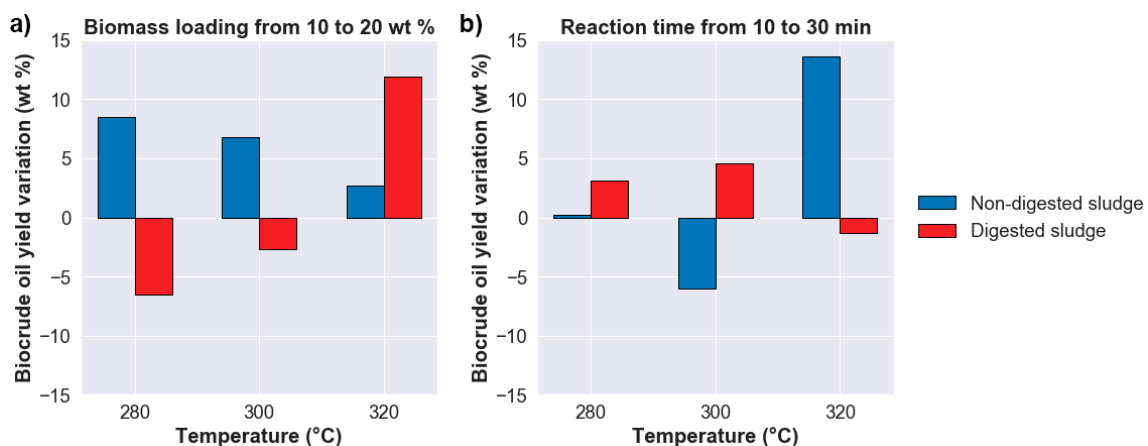
286

287 **Figure 1** – Comparison of the HTL product yields (dry, ash-free basis) for (a) biocrude oil, (b)
 288 hydrochar; and (c) gas. Results are obtained by converting non-digested and digested sludges
 289 at different HTL conditions: reaction time of 10 min and biomass loading of 10 wt %; reaction
 290 time of 10 min and biomass loading of 20 wt %; and reaction time of 30 min and biomass
 291 loading of 20 wt %.

292 *Effect of biomass loading:* the highest biocrude oil yields were obtained for both types of
 293 sludge at a biomass loading of 20 wt %. In the case of non-digested sludge, increasing the
 294 biomass loading from 10 to 20 wt % (reaction time of 10 min) increased the biocrude oil yield
 295 at all the conditions (**Figure 2a**), although this was more noticeable at low temperatures. The
 296 trend was different for digested sludge: increasing the biomass loading to 20 wt % decreased

297 the biocrude oil yield at 280 °C and 300 °C, and only increased it at 320 °C (albeit in a sharp
 298 manner, from 15.8 ± 0.5 to 27.7 ± 3.4 wt %). The reason for the reduced biocrude oil yield at
 299 280 °C and 300 °C could be related again to the more recalcitrant character of digested sludge,
 300 which likely requires higher temperatures (in this case, 320 °C) for biomass breakdown and
 301 biocrude oil formation under HTL conditions.

302 An increase in the biocrude oil yields at higher biomass loading has been described for
 303 various types of biomass [33,60]. This effect was attributed to the behavior of small water-
 304 soluble organic products that form during early stages of HTL. These products can undergo
 305 repolymerization reactions with a reaction order higher than 1 to form biocrude oil [33], which
 306 implies that such reactions are enhanced at increased biomass loadings. This is enhanced in
 307 batch reactors like the one used in this study, where no dilution takes place due to mixing.
 308 However, this does not mean that higher biomass loadings above 20 wt % will necessarily lead
 309 to even higher biocrude oil yields. Water acts as a reactant during HTL, and several literature
 310 studies indicated that high biomass loading could decrease the biocrude oil formation due to
 311 insufficient availability of the solvent (in this case, water) for stabilizing and dissolving the
 312 biomass [61,62].



313
 314 **Figure 2** – Variation of the biocrude oil yields for non-digested and digested sludge by
 315 modifying the HTL conditions. (a) Biocrude oil yield difference at biomass loadings of 10 and

316 20 wt % (reaction time of 10 min). (b) Biocrude oil yield difference at reaction times of 10 and
317 30 min (biomass loading of 20 wt %).

318 *Effect of reaction time:* The highest biocrude oil yield was attained using non-digested
319 sludge with a reaction time of 30 min (41.0 ± 0.3 wt %, as opposed to 27.4 ± 4.1 wt % at the
320 same conditions but 10 min), but this trend did not hold for all the conditions tested (**Figure**
321 **2b**). In fact, the highest biocrude oil yield for digested sludge was achieved with just 10 min.
322 The data shown here seems to indicate that extending the reaction time at 320 °C favored
323 biocrude oil formation reactions for non-digested sludge (**Figure 1a**), whereas degradation
324 reactions to form gas were promoted at that temperature for digested sludge (**Figure 1c**).

325 **3.2.DFT calculations**

326 Asphaltenes are large polycyclic aromatic molecules present in fossil asphalt that are key
327 for the mechanical performance of asphalt binder. While it is envisaged that the entire biocrude
328 oil mass would be used as additive for asphalt [9,14,19,20], it is also important to understand
329 how the asphaltenes in biocrude oil behave at the nanoscale and how this affects the
330 mechanical performance, cracking resistance and infrastructure durability of asphalt concrete.
331 Asphaltene-like matter can constitute up to 30 wt % in biocrude oils, depending on the biomass
332 source and the HTL conditions applied [24,63]. Previous work from our group [27] showed
333 that biobased asphaltenes had a higher content of heteroatoms than fossil asphaltenes. This
334 high heteroatomic content can lead to undesired properties, including high acidity,
335 polymerization, or increased viscosity and poor mechanical behavior upon aging [31,64], but
336 also rejuvenating properties, or lower temperature applicability [14,19]. To investigate these
337 issues and potential benefits, we performed DFT calculations to analyze at the molecular level
338 the differences in thermodynamic stability and aggregation tendency between fossil and
339 biobased asphaltenes (**Figure S2**), and we calculated conceptual DFT reactivity descriptors to
340 understand biocrude aging in asphaltene clusters. Such fundamental investigations are a

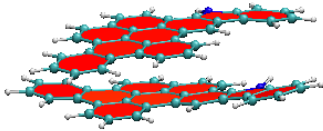
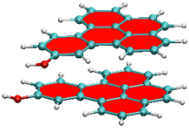
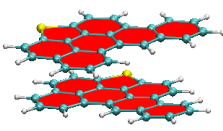
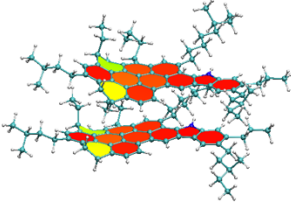
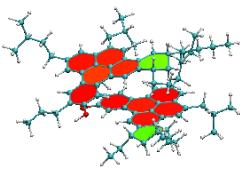
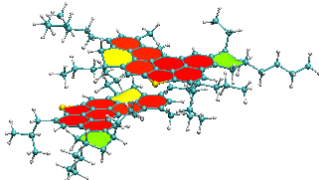
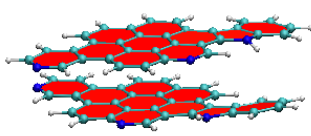
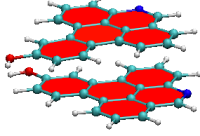
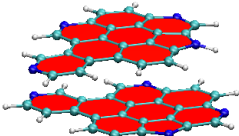
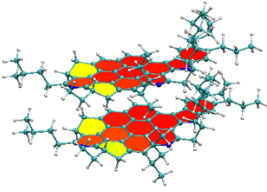
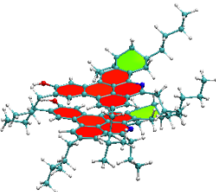
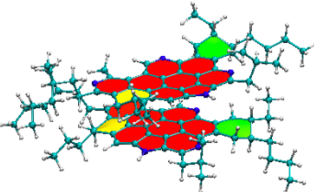
341 valuable tool to guide the HTL process conditions towards the production of biocrude oils with
342 optimal chemical features in asphalt mixtures. For a discussion about the role of other
343 compounds from biocrude oil (like amines or amides), the reader is referred elsewhere
344 [14,19,65].

345 Hardening and crack formation in asphalt pavements is associated to the formation of larger
346 clusters of asphaltene molecules and supramolecular nanoaggregates due to oxidative aging [14].
347 The increase in the number of these nanoaggregates unbalances the cluster/matrix ratio in the
348 asphalt mixtures, leading to a loss of flexibility and consequently hardening the material at the
349 macroscopic scale. We selected dimer structures of asphaltenes as a reasonable model system to
350 study the differences in aggregation tendency between fossil and biobased asphaltenes. The
351 model systems selected allowed us to isolate the effect of π - π interactions between the aromatic
352 cores, while minimizing the steric hindrance associated with peripheral aliphatic chains.
353 Furthermore, we compared structures with and without peripheral aliphatic chains to also assess
354 the relative importance of the aromatic cores and the aliphatic side chains on the interaction and
355 stabilization of the dimers. **Table 1** show the DFT-optimized structures and binding energies for
356 fossil and biobased asphaltene dimers, representing their most thermodynamically stable
357 conformation. The planarity of the rings in the aromatic core (closely related to their aromatic
358 character) is color-coded: most planar rings, expected to be more aromatic, are displayed in red
359 and orange, whereas yellow and green rings highly deviate from planarity (i.e., non-aromatic
360 rings). The DFT-optimized dimer structures revealed a similar ratio of planar and non-planar
361 rings for both fossil and biobased asphaltenes, which implies that the aromaticity is similar for
362 both types of asphaltenes. A similar aromaticity implies similar π - π stacking mechanisms, which
363 suggests the formations of similar nanoaggregates to those described in the Yen-Mullins model
364 for fossil asphaltenes. This also hinted at a similar stiffness of the polycyclic aromatic cores,
365 despite the higher content of heteroatoms of the biobased ones. Aromatic cores of asphaltenes

366 (without aliphatic chains) revealed a marginally more negative binding energy for biobased
367 asphaltenes (0.6 to 2.2 kcal/mol lower), attributed to their higher content of heteroatoms. In
368 particular, the presence of nitrogen is expected to boost the π system of electrons due to nitrogen
369 lone electron pairs, therefore contributing to stronger π - π interactions. However, this stronger
370 interaction did not lead to a reduced intermolecular distance. In fact, biobased asphaltenes
371 displayed intermolecular distances d 0.12-0.20 Å larger than fossil asphaltenes.

372 The situation changed when considering aliphatic side chains, as they reduced the π - π
373 interactions between the asphaltenes cores. The steric hindrance caused by the side chains
374 increased the distance between geometric centers (d) of aromatic cores. Furthermore, the
375 polarization of electron density redistribution (an additional intermolecular force between
376 asphaltenes discussed later with the dipolar moment) was also enhanced by higher content of
377 heteroatoms. This agreed with earlier experimental work showing a higher complex modulus for
378 HTL biocrude oils, compared to standard bitumen [8]. The reduced sliding in biobased
379 asphaltenes was attributed to their higher content of heteroatoms in biocrude oils, which
380 appeared to stabilize the intermolecular interactions. This was reflected in the intermolecular
381 distance d between aromatic cores (d), which was lower for biobased asphaltenes. The shorter
382 π - π stacking distance d of biobased asphaltenes hinted at a higher stability (more negative E_{bind})
383 of these dimers. This was confirmed by calculating the ratio of interaction energies with and
384 without peripheral aliphatic chains: in the case of fossil asphaltenes, the interaction energy
385 without aliphatic chains corresponded to 56.7-74.0% of that of structures with aliphatic chains.
386 In the case of biobased asphaltenes, the contribution increased to 72.7-87.2%. A seemingly
387 counterintuitive result was obtained for systems with aliphatic chains, which led to more negative
388 binding energies despite their increase in the distance between the aromatic cores due to the
389 steric hindrance. Based on earlier studies, we attributed this effect to aliphatic chains, which
390 interacted via van der Waals interactions to stabilize the asphaltene aggregates [29,66].

391 **Table 1** – Binding energy (E_{bind}) and distance between geometric centers of aromatic cores (d)
 392 for fossil and biobased asphaltenes. Several starting geometries were investigated for each
 393 dimer. Only the lowest energy conformation is displayed here.

Fossil asphaltenes			
<i>Without aliphatic chains</i>			
			
E_{bind} (kcal/mol)	-19.0	-9.7	-15.0
d (Å)	3.17	3.52	3.36
<i>With aliphatic chains</i>			
			
E_{bind} (kcal/mol)	-25.7	-17.1	-20.3
d (Å)	5.60	4.34	6.93
Biobased asphaltenes			
<i>Without aliphatic chains</i>			
			
E_{bind} (kcal/mol)	-21.2	-10.6	-15.6
d (Å)	3.35	3.72	3.48
<i>With aliphatic chains</i>			
			

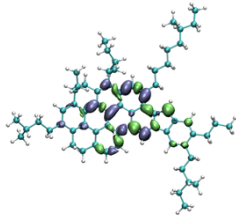
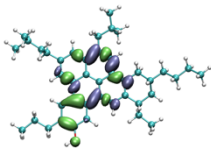
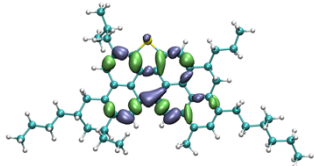
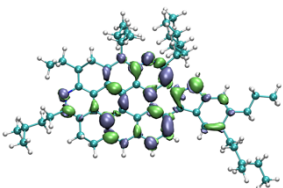
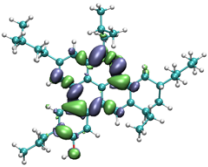
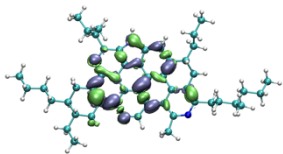
E_{bind} (kcal/mol)	-24.3	-14.5	-21.4
d (Å)	5.14	4.22	3.91

394

395 **Table 2** shows the reactivity analysis using conceptual DFT reactivity descriptors, as well
396 as the calculations of the dipole moment for individual molecules. The results confirmed the
397 higher polarization induced by heteroatoms in biobased asphaltenes: their dipole moment was
398 more than three times larger than for fossil asphaltenes. It should be noted that other dimer
399 conformations, which may exist but not have been considered in this study, could be more
400 largely affected by heteroatoms and have a larger important role in π - π stacking due to their
401 effect on the π electron distributions of the asphaltene aromatic core. The larger dipole moment
402 could play a role in cluster-to-cluster interactions, influencing the formation of supramolecular
403 structures and cluster aggregates, as described in the Yen-Mullins model for asphalt [22]. Even
404 though asphaltenes are flexible molecules, we believe that the dipole moment is a good metric
405 to compare fossil and biobased asphaltenes in a static approach. Future work should assess if a
406 more dynamic description of their polar character (e.g., polarizability or molecular polarity
407 index calculations) would provide different outcomes. Moreover, the values for the global
408 chemical hardness showed that fossil asphaltenes were more reactive than biobased
409 asphaltenes. This indicated that biocrude oils could act as antioxidant additives in asphalt
410 binder [29], preventing oxidation events that eventually lead to pavement cracking.

411 Finally, the dual descriptor of the Fukui function revealed the favorable molecular regions
412 for a nucleophilic or electrophilic attack. To date, there is no significant evidence of the
413 oxidation mechanisms of asphaltene molecules. On the one hand, if a nucleophilic and
414 electrophilic reaction takes place, the dual descriptor of the Fukui function indicates the areas
415 where such reactions would happen. On the other hand, if the oxidation mechanism follows a
416 radical reaction, the dual descriptor of the Fukui function helps to identify the most reactive

417 **Table 2** – Chemical hardness (η), total dipole moment (D), and the dual descriptor of the
 418 Fukui function for fossil and biobased asphaltenes (plotted at isosurface values of 0.001
 419 electron-bohr⁻³). Green surfaces in the dual descriptor of the Fukui function indicate areas
 420 that are suitable to undergo electrophilic attack upon chemical reaction. Purple surfaces
 421 indicate areas that are suitable to undergo nucleophilic attack upon chemical reaction.

Fossil asphaltenes			
Fukui function (dual descriptor)			
η (eV)	1.69	1.93	1.57
D (Debye)	1.92	1.64	1.30
Biobased asphaltenes			
Fukui function (dual descriptor)			
η (eV)*	2.68	3.14	3.00
D (Debye)	3.69	3.54	5.42

422 *This values are taken from López Barreiro et al [27] for comparison to the fossil asphaltenes
 423 areas of the molecule where the initiation step could take place. This is because the Fukui
 424 function is directly connected to the localization of the frontier orbitals, and therefore to the
 425 place in the molecular structure where a radical electron could be generated. Studying the
 426 subsequent radical reaction would require calculating the spin density for the radical electrons.
 427 However, the detailed mechanism of an oxidative radical process is beyond the scope of this
 428 work. Regardless of the mechanisms, the results showed similar local reactivity for fossil and

429 biobased asphaltenes, with the reactive centers mostly localized in the polycyclic aromatic
430 cores.

431 **4. CONCLUSION**

432 In this work we explored the effect of different process parameters (feedstock type,
433 temperature, reaction time, and biomass loading) on the yields of biocrude oils obtained from
434 HTL of sewage sludge, and we provided an atomistic description of the aggregation
435 mechanisms and the reactivity of biobased and fossil asphaltene molecules. On the one hand,
436 the experimental results indicated that non-digested sewage sludge led to higher biocrude oil
437 yields, with optimal temperatures at 300-320 °C, using biomass loadings of 20 wt %. On the
438 other hand, DFT calculations indicated similar thermodynamic stability for both biocrude and
439 fossil asphaltene molecules, despite the higher heteroatomic content in the biobased ones. The
440 intermolecular π - π stacking distance between the geometric center of aromatic cores was
441 slightly lower for biobased asphaltenes. Taken together, these computational results suggest
442 similar clustering and supramolecular aggregation mechanisms for both biocrude and fossil
443 asphaltenes, which sets some theoretical foundation for the development of a general model for
444 biocrude oils, analogous to the Yen-Mullins model of asphalt. Our results agree with earlier
445 experimental data reporting a similar rheology profile for standard bitumen and HTL biocrude
446 oils, with a slightly higher complex modulus for the later. Overall, this work contributes to
447 advance the utilization of HTL biocrude oils in the asphalt pavement industry, both from the
448 process engineering and the application perspectives.

449 **ACKNOWLEDGEMENTS**

450 MITEI, Ferrovial and Cadagua are acknowledged for the financial support of this research.
451 Computational calculations were performed on the MIT Engaging Cluster (funded by DoD-
452 DURIP) and the Extreme Science and Engineering Discovery Environment (XSEDE) which is
453 supported by the National Science Foundation grant number TG-MSS090007. F.M.-M.

454 acknowledges the support of the computational resources from Supercomputing Wales and
455 Google Cloud Platform.

456 **SUPPORTING INFORMATION**

457 WWTP scheme, chemical structures for fossil and biobased asphaltenes, sewage sludge
458 proximate analysis and HTL yields.

459 **REFERENCES**

- 460 [1] W.-T. Chen, M.A. Haque, T. Lu, A. Aierzhati, G. Reimonn, A perspective on
461 hydrothermal processing of sewage sludge, *Curr. Opin. Environ. Sci. Heal.* 14 (2020)
462 63–73. <https://doi.org/https://doi.org/10.1016/j.coesh.2020.02.008>.
- 463 [2] L. Snowden-Swan, Y. Zhu, S. Jones, D. Elliott, A. Schmidt, R. Hallen, J. Billing, T.
464 Hart, S. Fox, G. Maupin, *Hydrothermal Liquefaction and Upgrading of Municipal
465 Wastewater Treatment Plant Sludge: A Preliminary Techno-Economic Analysis*, 2016.
- 466 [3] J. Mateo-Sagasta, L. Raschid-Sally, A. Thebo, *Global Wastewater and Sludge
467 Production, Treatment and Use BT - Wastewater: Economic Asset in an Urbanizing
468 World*, in: P. Drechsel, M. Qadir, D. Wichelns (Eds.), Springer Netherlands, Dordrecht,
469 2015: pp. 15–38. https://doi.org/10.1007/978-94-017-9545-6_2.
- 470 [4] C. Rodriguez Correa, M. Bernardo, R.P.P.L. Ribeiro, I.A.A.C. Esteves, A. Kruse,
471 Evaluation of hydrothermal carbonization as a preliminary step for the production of
472 functional materials from biogas digestate, *J. Anal. Appl. Pyrolysis.* 124 (2017) 461–
473 474. <https://doi.org/https://doi.org/10.1016/j.jaap.2017.02.014>.
- 474 [5] EAPA, *Asphalt in Figures 2020*, 2020. <https://eapa.org/asphalt-in-figures/>.
- 475 [6] I. Gonzalez-Torre, J. Norambuena-Contreras, Recent advances on self-healing of
476 bituminous materials by the action of encapsulated rejuvenators, *Constr. Build. Mater.*

- 477 258 (2020) 119568. <https://doi.org/10.1016/j.conbuildmat.2020.119568>.
- 478 [7] M. Southern, A perspective of bituminous binder specifications, Elsevier Ltd., 2015.
479 <https://doi.org/10.1016/B978-0-08-100269-8.00001-5>.
- 480 [8] C. Geantet, D. Laurenti, N. Guilhaume, C. Lorentz, I. Borghol, B. Bujoli, E. Chailleux,
481 R. Checa, S. Schramm, V. Carré, F. Aubriet, C. Queffélec, FT-ICR MS characterization
482 of bio-binders for road pavement from HTL of microalgae residues, *J. Environ. Chem.*
483 *Eng.* 10 (2022). <https://doi.org/10.1016/j.jece.2022.107361>.
- 484 [9] M. Audo, M. Paraschiv, C. Queffélec, I. Louvet, J. Hémez, F. Fayon, O. Lépine, J.
485 Legrand, M. Tazerout, E. Chailleux, B. Bujoli, Subcritical Hydrothermal Liquefaction of
486 Microalgae Residues as a Green Route to Alternative Road Binders, *ACS Sustain.*
487 *Chem. Eng.* 3 (2015) 583–590. <https://doi.org/10.1021/acssuschemeng.5b00088>.
- 488 [10] E. Chailleux, M. Audo, S. Goyer, C. Queffelec, O. Marzouk, Advances in the
489 development of alternative binders from biomass for the production of biosourced road
490 binders, Elsevier Ltd., 2015. <https://doi.org/10.1016/B978-0-08-100269-8.00011-8>.
- 491 [11] D.R. Vardon, B.K. Sharma, J. Scott, G. Yu, Z. Wang, L. Schideman, Y. Zhang, T.J.
492 Strathmann, Chemical properties of biocrude oil from the hydrothermal liquefaction of
493 *Spirulina* algae, swine manure, and digested anaerobic sludge, *Bioresour. Technol.* 102
494 (2011) 8295–8303. <https://doi.org/https://doi.org/10.1016/j.biortech.2011.06.041>.
- 495 [12] D.C. Elliott, P. Biller, A.B. Ross, A.J. Schmidt, S.B. Jones, Hydrothermal liquefaction
496 of biomass: Developments from batch to continuous process, *Bioresour. Technol.* 178
497 (2015) 147–156. <https://doi.org/https://doi.org/10.1016/j.biortech.2014.09.132>.
- 498 [13] D. López Barreiro, M. Beck, U. Hornung, F. Ronsse, A. Kruse, W. Prins, Suitability of
499 hydrothermal liquefaction as a conversion route to produce biofuels from macroalgae,

- 500 Algal Res. 11 (2015). <https://doi.org/10.1016/j.algal.2015.06.023>.
- 501 [14] F. Pahlavan, A. Rajib, S. Deng, P. Lammers, E.H. Fini, Investigation of Balanced
502 Feedstocks of Lipids and Proteins To Synthesize Highly Effective Rejuvenators for
503 Oxidized Asphalt, ACS Sustain. Chem. Eng. 8 (2020) 7656–7667.
504 <https://doi.org/10.1021/acssuschemeng.0c01100>.
- 505 [15] A.A. Peterson, F. Vogel, R.P. Lachance, M. Fröling, M.J. Antal, Jr., J.W. Tester,
506 Thermochemical biofuel production in hydrothermal media: A review of sub- and
507 supercritical water technologies, Energy Environ. Sci. 1 (2008) 32–65.
508 <https://doi.org/10.1039/B810100K>.
- 509 [16] A. Kruse, N. Dahmen, Water – A magic solvent for biomass conversion, J. Supercrit.
510 Fluids. 96 (2015) 36–45. <https://doi.org/https://doi.org/10.1016/j.supflu.2014.09.038>.
- 511 [17] T.E. Seiple, R.L. Skaggs, L. Fillmore, A.M. Coleman, Municipal wastewater sludge as a
512 renewable, cost-effective feedstock for transportation biofuels using hydrothermal
513 liquefaction, J. Environ. Manage. 270 (2020) 110852.
514 <https://doi.org/https://doi.org/10.1016/j.jenvman.2020.110852>.
- 515 [18] R. Amoedo, T. Damartzis, J. Granacher, F. Marechal, System Design and Performance
516 Evaluation of Wastewater Treatment Plants Coupled With Hydrothermal Liquefaction
517 and Gasification, Front. Energy Res. 8 (2020) 233.
518 <https://doi.org/10.3389/fenrg.2020.568465>.
- 519 [19] F. Pahlavan, A. Samieadel, S. Deng, E. Fini, Exploiting Synergistic Effects of
520 Intermolecular Interactions To Synthesize Hybrid Rejuvenators To Revitalize Aged
521 Asphalt, ACS Sustain. Chem. Eng. 7 (2019) 15514–15525.
522 <https://doi.org/10.1021/acssuschemeng.9b03263>.

- 523 [20] Z.Y. Mahssin, M.M. Zainol, N.A. Hassan, H. Yaacob, M.H. Puteh, N.A. Saidina Amin,
524 Hydrothermal liquefaction bioproduct of food waste conversion as an alternative
525 composite of asphalt binder, *J. Clean. Prod.* 282 (2021).
526 <https://doi.org/10.1016/j.jclepro.2020.125422>.
- 527 [21] R. Zhang, H. Wang, Z. You, X. Jiang, X. Yang, Optimization of bio-asphalt using bio-
528 oil and distilled water, *J. Clean. Prod.* 165 (2017) 281–289.
529 <https://doi.org/10.1016/j.jclepro.2017.07.154>.
- 530 [22] O.C. Mullins, The Modified Yen Model, *Energy & Fuels.* 24 (2010) 2179–2207.
531 <https://doi.org/10.1021/ef900975e>.
- 532 [23] Z. Yang, X. Zhang, Z. Zhang, B. Zou, Z. Zhu, G. Lu, W. Xu, J. Yu, H. Yu, Effect of
533 aging on chemical and rheological properties of bitumen, *Polymers (Basel).* 10 (2018).
534 <https://doi.org/10.3390/polym10121345>.
- 535 [24] C. Torri, L. Garcia Alba, C. Samorì, D. Fabbri, D.W.F. (Wim) Brilman, Hydrothermal
536 Treatment (HTT) of Microalgae: Detailed Molecular Characterization of HTT Oil in
537 View of HTT Mechanism Elucidation, *Energy & Fuels.* 26 (2012) 658–671.
538 <https://doi.org/10.1021/ef201417e>.
- 539 [25] S. Bjelić, J. Yu, B.B. Iversen, M. Glasius, P. Biller, Detailed Investigation into the
540 Asphaltene Fraction of Hydrothermal Liquefaction Derived Bio-Crude and Hydrotreated
541 Bio-Crudes, *Energy and Fuels.* 32 (2018) 3579–3587.
542 <https://doi.org/10.1021/acs.energyfuels.7b04119>.
- 543 [26] G. Robertson, K.V. Adiningtyas, S.A. Ebrahim, L. Scoles, E.A. Baranova, D. Singh,
544 Understanding the nature of bio-asphaltenes produced during hydrothermal liquefaction,
545 *Renew. Energy.* 173 (2021) 128–140. <https://doi.org/10.1016/j.renene.2021.03.099>.

- 546 [27] D. López Barreiro, F.J. Martin-Martinez, C. Torri, W. Prins, M.J. Buehler, Molecular
547 characterization and atomistic model of biocrude oils from hydrothermal liquefaction of
548 microalgae, *Algal Res.* 35 (2018). <https://doi.org/10.1016/j.algal.2018.08.034>.
- 549 [28] P. Geerlings, F. De Proft, W. Langenaeker, Conceptual Density Functional Theory,
550 *Chem. Rev.* 103 (2003) 1793–1874. <https://doi.org/10.1021/cr990029p>.
- 551 [29] M. Mousavi, F. Pahlavan, D. Oldham, S. Hosseinneshad, E.H. Fini, Multiscale
552 Investigation of Oxidative Aging in Biomodified Asphalt Binder, *J. Phys. Chem. C.* 120
553 (2016) 17224–17233. <https://doi.org/10.1021/acs.jpcc.6b05004>.
- 554 [30] D. López Barreiro, W. Prins, F. Ronsse, W. Brilman, Hydrothermal liquefaction (HTL)
555 of microalgae for biofuel production: State of the art review and future prospects,
556 *Biomass and Bioenergy.* 53 (2013). <https://doi.org/10.1016/j.biombioe.2012.12.029>.
- 557 [31] H. Dhasmana, H. Ozer, I.L. Al-Qadi, Y. Zhang, L. Schideman, B.K. Sharma, W.-T.
558 Chen, M.J. Minarick, P. Zhang, Rheological and Chemical Characterization of
559 Biobinders from Different Biomass Resources, *Transp. Res. Rec.* 2505 (2015) 121–129.
560 <https://doi.org/10.3141/2505-16>.
- 561 [32] L. Garcia Alba, C. Torri, C. Samorì, J. van der Spek, D. Fabbri, S.R.A. Kersten, D.W.F.
562 (Wim) Brilman, Hydrothermal Treatment (HTT) of Microalgae: Evaluation of the
563 Process As Conversion Method in an Algae Biorefinery Concept, *Energy & Fuels.* 26
564 (2012) 642–657. <https://doi.org/10.1021/ef201415s>.
- 565 [33] A. Kruse, M. Faquir, Hydrothermal Biomass Gasification – Effects of Salts, Backmixing
566 and Their Interaction, *Chem. Eng. Technol.* 30 (2007) 749–754.
567 <https://doi.org/https://doi.org/10.1002/ceat.200600409>.
- 568 [34] F. Neese, The ORCA program system, *WIREs Comput. Mol. Sci.* 2 (2012) 73–78.

- 569 <https://doi.org/https://doi.org/10.1002/wcms.81>.
- 570 [35] D.D. Li, M.L. Greenfield, Chemical compositions of improved model asphalt systems
571 for molecular simulations, *Fuel*. 115 (2014) 347–356.
572 <https://doi.org/https://doi.org/10.1016/j.fuel.2013.07.012>.
- 573 [36] F.J. Martín-Martínez, E.H. Fini, M.J. Buehler, Molecular asphaltene models based on
574 Clar sextet theory, *RSC Adv.* 5 (2015) 753–759. <https://doi.org/10.1039/C4RA05694A>.
- 575 [37] B. Schuler, Y. Zhang, F. Liu, A.E. Pomerantz, A.B. Andrews, L. Gross, V. Pauchard, S.
576 Banerjee, O.C. Mullins, Overview of Asphaltene Nanostructures and Thermodynamic
577 Applications, *Energy & Fuels*. 34 (2020) 15082–15105.
578 <https://doi.org/10.1021/acs.energyfuels.0c00874>.
- 579 [38] A.A. Shah, S.S. Toor, F. Conti, A.H. Nielsen, L.A. Rosendahl, Hydrothermal
580 liquefaction of high ash containing sewage sludge at sub and supercritical conditions,
581 *Biomass and Bioenergy*. 135 (2020). <https://doi.org/10.1016/j.biombioe.2020.105504>.
- 582 [39] D. Castello, M.S. Haider, L.A. Rosendahl, Catalytic upgrading of hydrothermal
583 liquefaction biocrudes: Different challenges for different feedstocks, *Renew. Energy*.
584 141 (2019) 420–430. <https://doi.org/10.1016/j.renene.2019.04.003>.
- 585 [40] W. Zhang, Y. Liang, Hydrothermal liquefaction of sewage sludge – effect of four
586 reagents on relevant parameters related to biocrude and PFAS, *J. Environ. Chem. Eng.*
587 10 (2022). <https://doi.org/10.1016/j.jece.2021.107092>.
- 588 [41] C. Corminboeuf, Minimizing Density Functional Failures for Non-Covalent Interactions
589 Beyond van der Waals Complexes, *Acc. Chem. Res.* 47 (2014) 3217–3224.
590 <https://doi.org/10.1021/ar400303a>.
- 591 [42] S. Grimme, J. Antony, S. Ehrlich, H. Krieg, A consistent and accurate ab initio

- 592 parametrization of density functional dispersion correction (DFT-D) for the 94 elements
593 H-Pu, *J. Chem. Phys.* 132 (2010) 154104. <https://doi.org/10.1063/1.3382344>.
- 594 [43] S. Grimme, S. Ehrlich, L. Goerigk, Effect of the damping function in dispersion
595 corrected density functional theory, *J. Comput. Chem.* 32 (2011) 1456–1465.
596 <https://doi.org/https://doi.org/10.1002/jcc.21759>.
- 597 [44] H. Kruse, S. Grimme, A geometrical correction for the inter- and intra-molecular basis
598 set superposition error in Hartree-Fock and density functional theory calculations for
599 large systems, *J. Chem. Phys.* 136 (2012) 154101. <https://doi.org/10.1063/1.3700154>.
- 600 [45] M. Mousavi, T. Abdollahi, F. Pahlavan, E.H. Fini, The influence of asphaltene-resin
601 molecular interactions on the colloidal stability of crude oil, *Fuel*. 183 (2016) 262–271.
602 <https://doi.org/https://doi.org/10.1016/j.fuel.2016.06.100>.
- 603 [46] R.G. Parr, R.G. Pearson, Absolute hardness: companion parameter to absolute
604 electronegativity, *J. Am. Chem. Soc.* 105 (1983) 7512–7516.
605 <https://doi.org/10.1021/ja00364a005>.
- 606 [47] C. Cárdenas, P. Ayers, F. De Proft, D.J. Tozer, P. Geerlings, Should negative electron
607 affinities be used for evaluating the chemical hardness?, *Phys. Chem. Chem. Phys.* 13
608 (2011) 2285–2293. <https://doi.org/10.1039/C0CP01785J>.
- 609 [48] W. Humphrey, A. Dalke, K. Schulten, VMD: Visual molecular dynamics, *J. Mol.*
610 *Graph.* 14 (1996) 33–38. [https://doi.org/10.1016/0263-7855\(96\)00018-5](https://doi.org/10.1016/0263-7855(96)00018-5).
- 611 [49] D. Cremer, J.A. Pople, General definition of ring puckering coordinates, *J. Am. Chem.*
612 *Soc.* 97 (1975) 1354–1358. <https://doi.org/10.1021/ja00839a011>.
- 613 [50] S. Brand, F. Hardi, J. Kim, D.J. Suh, Effect of heating rate on biomass liquefaction:
614 Differences between subcritical water and supercritical ethanol, *Energy*. 68 (2014) 420–

- 615 427. <https://doi.org/https://doi.org/10.1016/j.energy.2014.02.086>.
- 616 [51] F. Behrendt, Y. Neubauer, M. Oevermann, B. Wilmes, N. Zobel, Direct Liquefaction of
617 Biomass, (2008) 667–677. <https://doi.org/10.1002/ceat.200800077>.
- 618 [52] T. Ogi, S. Yokoyama, K. Koguchi, Direct liquefaction of wood by alkaly and alkaline
619 earth salt in an aqueous phase, *Chem. Lett.* 14 (1985) 1199–1202.
620 <https://doi.org/10.1246/cl.1985.1199>.
- 621 [53] S. Karagöz, T. Bhaskar, A. Muto, Y. Sakata, Hydrothermal upgrading of biomass:
622 Effect of K₂CO₃ concentration and biomass/water ratio on products distribution,
623 *Bioresour. Technol.* 97 (2006) 90–98.
624 <https://doi.org/https://doi.org/10.1016/j.biortech.2005.02.051>.
- 625 [54] M. Schumacher, J. Yanik, A. Sinağ, A. Kruse, Hydrothermal conversion of seaweeds in
626 a batch autoclave, *J. Supercrit. Fluids.* 58 (2011) 131–135.
627 <https://doi.org/https://doi.org/10.1016/j.supflu.2011.04.009>.
- 628 [55] U. Jena, K.C. Das, J.R. Kastner, Comparison of the effects of Na₂CO₃, Ca₃(PO₄)₂, and
629 NiO catalysts on the thermochemical liquefaction of microalga *Spirulina platensis*,
630 *Appl. Energy.* 98 (2012) 368–375.
631 <https://doi.org/https://doi.org/10.1016/j.apenergy.2012.03.056>.
- 632 [56] J. Schuler, U. Hornung, A. Kruse, N. Dahmen, J. Sauer, Hydrothermal Liquefaction of
633 Lignin, *J. Biomater. Nanobiotechnol.* 8 (2017) 96–108.
- 634 [57] D. López Barreiro, C. Samorì, G. Terranella, U. Hornung, A. Kruse, W. Prins, Assessing
635 microalgae biorefinery routes for the production of biofuels via hydrothermal
636 liquefaction, *Bioresour. Technol.* 174 (2014).
637 <https://doi.org/10.1016/j.biortech.2014.10.031>.

- 638 [58] D. Xu, G. Lin, L. Liu, Y. Wang, Z. Jing, S. Wang, Comprehensive evaluation on
639 product characteristics of fast hydrothermal liquefaction of sewage sludge at different
640 temperatures, *Energy*. 159 (2018) 686–695.
641 <https://doi.org/https://doi.org/10.1016/j.energy.2018.06.191>.
- 642 [59] X. Zhang, X. Li, R. Li, Y. Wu, Hydrothermal Carbonization and Liquefaction of Sludge
643 for Harmless and Resource Purposes: A Review, *Energy & Fuels*. 34 (2020) 13268–
644 13290. <https://doi.org/10.1021/acs.energyfuels.0c02467>.
- 645 [60] D. Lopez Barreiro, B.R. Gómez, U. Hornung, A. Kruse, W. Prins, Hydrothermal
646 Liquefaction of Microalgae in a Continuous Stirred-Tank Reactor, *Energy and Fuels*. 29
647 (2015). <https://doi.org/10.1021/acs.energyfuels.5b02099>.
- 648 [61] S. Zou, Y. Wu, M. Yang, J. Tong, Bio-oil production from sub- and supercritical water
649 liquefaction of microalgae *Dunaliella tertiolecta* and related properties, (2010) 1073–
650 1078. <https://doi.org/10.1039/c002550j>.
- 651 [62] H. Huang, X. Yuan, G. Zeng, J. Wang, H. Li, C. Zhou, X. Pei, Q. You, L. Chen,
652 Thermochemical liquefaction characteristics of microalgae in sub- and supercritical
653 ethanol, *Fuel Process. Technol.* 92 (2011) 147–153.
654 <https://doi.org/10.1016/j.fuproc.2010.09.018>.
- 655 [63] C. Torri, D. López Barreiro, R. Conti, D. Fabbri, W. Brilman, Fast Procedure for the
656 Analysis of Hydrothermal Liquefaction Biocrude with Stepwise Py-GC-MS and Data
657 Interpretation Assisted by Means of Non-negative Matrix Factorization, *Energy and*
658 *Fuels*. 30 (2016). <https://doi.org/10.1021/acs.energyfuels.5b02688>.
- 659 [64] S. Lv, X. Peng, C. Liu, F. Qu, X. Zhu, W. Tian, J. Zheng, Aging resistance evaluation of
660 asphalt modified by Buton-rock asphalt and bio-oil based on the rheological and
661 microscopic characteristics, *J. Clean. Prod.* 257 (2020) 120589.

- 662 <https://doi.org/https://doi.org/10.1016/j.jclepro.2020.120589>.
- 663 [65] A.M. Hung, M. Mousavi, F. Pahlavan, E.H. Fini, Intermolecular Interactions of Isolated
664 Bio-Oil Compounds and Their Effect on Bitumen Interfaces, *ACS Sustain. Chem. Eng.*
665 5 (2017) 7920–7931. <https://doi.org/10.1021/acssuschemeng.7b01462>.
- 666 [66] T. Takanohashi, S. Sato, I. Saito, R. Tanaka, Molecular dynamics simulation of the heat-
667 induced relaxation of asphaltene aggregates, *Energy and Fuels*. 17 (2003) 135–139.
668 <https://doi.org/10.1021/ef0201275>.
- 669